ChemPubSoc Europe

DOI: 10.1002/ejic.201801374

EurJIC European Journal of Inorganic Chemistry

Full Paper

Nanoparticles for Oxygen Transfer | *Very Important Paper* |

VIP $CeO_{2-\delta}$-Modified $CuFe_2O_4$ with Enhanced Oxygen Transfer as Efficient Catalysts for Selective Oxidation of Fluorene under Mild Conditions

Xiubing Huang,*[a][‡] Peng Wang,[a][‡] Hean Zhang,[a] Zhengwei Guo,[a] Jijia Liu,[a] Guilong Lu,[a] Guangsheng Pang,[b] and Ge Wang*[a]

Abstract: The design of efficient catalysts for the selective oxidation of sp^3 C–H bond with air at low temperature is of great importance to the scientific and industrial community. In this work, we design a $CeO_{2-\delta}$ modified $CuFe_2O_4$ catalyst by a post-modification method for the selective oxidation of fluorene under an air atmosphere and N-hydroxyphthalimide (NHPI) at 60 °C. HRTEM results indicate that $CeO_{2-\delta}$ nanoclusters sized around 5 nm are successfully modified on the surface of $CuFe_2O_4$. XPS and H_2-TPR results show that $CeO_{2-\delta}$ modification would favor oxygen transfer at lower temperature due to the synergetic effect between $CuFe_2O_4$ and $CeO_{2-\delta}$ with rich Ce^{3+}/Ce^{4+} couples. The results demonstrate that $CuFe_2O_4$@$CeO_{2-\delta}$-0.05 with 4.20 wt.-% Ce present the best catalytic performance with 94 % conversion of fluorene and excellent reusability at least five times. It is anticipated that the modification of $CeO_{2-\delta}$ nanoclusters on the surface leads to increased oxygen activation and transfer to $CuFe_2O_4$, which favors the activation of NHPI to phthalimide-*N*-oxyl (PINO) radicals and exhibits an improved catalytic performance. Our results provide some guidance on the design of efficient catalysts by the surface modification strategy.

Introduction

Selective oxidation of saturated sp^3-hybrid C–H bonds has been recognized as one of the most fundamental processes for the production of valuable alcohols, ketones, and aldehydes with wide applications in the agricultural, domestic, and so on.[1] Generally, expensive inorganic oxidants (e.g., $KMnO_4$, $K_2Cr_2O_7$, sodium chlorite) are usually used in the industry for the selective oxidation of saturated C–H bonds, which often produce simultaneously a large amount of toxic waste.[2] With the increasing concerns of environmental protection and sustainable development, remarkable efforts have been made to the highly selective oxidation of sp^3 C–H bonds with high conversion under mild conditions (e.g., atmosphere pressure, low temperature, cheap and clean oxidants).

Up to now, various kinds of homogeneous catalysts have been developed for the selective oxidation of sp^3 C–H bonds, but the difficulty in the separation of products from the reaction mixture as well as the non-reusability limit the wide applications of homogeneous catalyst.[3] In the last decades, more and more attentions have been focused on the research and development of heterogeneous catalysts for the highly selective oxidation of sp^3 C–H bonds.[4] In the early state, peroxide-type oxidants such as *tert*-butylhydroperoxide (TBHP) or H_2O_2 were usually used to oxidize sp^3 C–H bonds with high conversion,[5] nevertheless tert-butanol formed as a side-product for TBHP needs additive separation while H_2O_2 is corrosive to equipment. Therefore, it is desirable to develop more efficient heterogeneous catalysts using environmentally friendly and economic pure oxygen or air as oxidant. Until now, some heterogeneous catalysts have been demonstrated to be active for the selective oxidation of saturated C–H bonds using molecule oxygen as oxidant.[6] For example, Dai et al. found that mesoporous $Mn_{0.5}Ce_{0.5}O_x$ solid solution was active for the selective oxidation of cyclohexane (12 h, conversion: 17.0 %, selectivity: 92 %) at 100 °C under 10 atm of O_2.[7] Hutchings et al. demonstrated that the oxidation of toluene could be realized using Au-Pd/C as catalyst at 160 °C under 10 atm of O_2 even though the conversion is only 4.4 % with 76.2 % selectivity after 7 h reaction.[8] But high O_2 pressure and high reaction temperature are often accompanied with uncontrolled conversion and/or selectivity due to the easy oxidation of their oxidized products. And the noble metal utilization also limits the practical applications. Although some photocatalysts (e.g., CdS,[9] VO@g-C_3N_4[10]) have been proven active for the selective oxidation of saturated sp^3 C–H bonds, their conversion is still relatively low. In substantial and green chemistry points of view, there is a strong research interest in the development of effective, eco-

[a] *Beijing Advanced Innovation Center for Materials Genome Engineering, Beijing Key Laboratory of Function Materials for Molecule & Structure Construction, School of Materials Science and Engineering, University of Science and Technology Beijing, Beijing, 100083, P. R. China*
E-mail: xiubinghuang@ustb.edu.cn
gewang@mater.ustb.edu.cn
http://www.nmclyjs-ustb.com/
[b] *State Key Laboratory of Inorganic Synthesis and Preparative Chemistry, College of Chemistry, Jilin University, Changchun, 130012, P. R. China*
[‡] Both the authors contributed equally to this work.
ORCID(s) from the author(s) for this article is/are available on the WWW under https://doi.org/10.1002/ejic.201801374.

nomical, and environmentally friendly heterogeneous catalysts using earth-abundant metals under mild reactions conditions (e.g., air, atmosphere pressure, low reaction temperature), however, which still represents critical challenges.

Among the heterogeneous catalysts, spinel oxides with the formula of AB_2O_4 containing 3d transition metal ions have been investigated as low-temperature catalyst for gas oxidation (e.g., CO, toluene),[11] liquid-phase alcohol oxidation,[12] because of their excellent catalytic activity, thermal stability, chemical stability, and easy recovery. Specially, copper-based spinel oxides have been investigated in the catalytic oxidation of VOCs,[13] synthesis of diaryl ethers[14] and steam reforming of methanol[15] at low temperature, even under ambient conditions due to their enhanced oxygen mobility and reducibility arose from the redox couples. However, the catalytic applications of copper-based spinel oxides in the liquid-phase selective oxidation of sp^3 C–H bonds under mild conditions have been rarely reported and demonstrated.[16] It has been reported that $CeO_{2-\delta}$ itself or $CeO_{2-\delta}$ modification on transition-metal oxides could improve the oxygen mobility at low temperature due to the high oxygen transfer proerty from the unique redox properties of Ce^{3+}/Ce^{4+},[17] however the synergetic interaction of $CeO_{2-\delta}$-modification between Cu-based spinel oxides during the catalytic process have been rarely reported. Herein, in this work, the catalytic activity of $CeO_{2-\delta}$-modified $CuFe_2O_4$ has been evaluated for the selective oxidation of fluorene at low temperature (60 °C) under air.

Results and Discussion

The XRD patterns of $CuFe_2O_4$ and $CuFe_2O_4$@$CeO_{2-\delta}$-*x* samples are shown in Figure 1. The results (Figure 1a) indicate that the position and relative intensity of diffraction peaks are in accordance with those of the tetragonally distorted inverse spinel $CuFe_2O_4$ (JCPDS 34–0425) and almost no impurity phases (e.g., CuO, Fe_2O_3) were observed. With the increasing amount of $CeO_{2-\delta}$, there are no obvious changes in the diffraction peaks of $CuFe_2O_4$ and the peaks for cubic $CeO_{2-\delta}$ are also not obvious except that there is a broad diffraction peak to the (111) crystal plane of $CeO_{2-\delta}$ in $CuFe_2O_4$@$CeO_{2-\delta}$-0.10 (Figure 1d) maybe due to the formation of $CeO_{2-\delta}$ small nanocrystals.

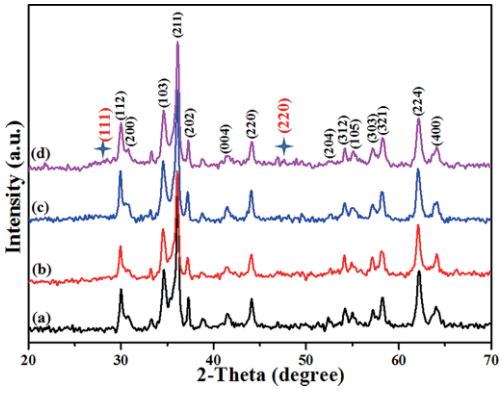

Figure 1. XRD patterns of (a) $CuFe_2O_4$, (b) $CuFe_2O_4$@$CeO_{2-\delta}$-0.025, (c) $CuFe_2O_4$@$CeO_{2-\delta}$-0.05, and (d) $CuFe_2O_4$@$CeO_{2-\delta}$-0.10.

The morphology and microstructure of as-prepared samples were demonstrated by TEM. From the TEM images with different magnifications (Figure 2a and Figure 2b), it can be clearly observed that $CuFe_2O_4$ exhibits the nanoparticle morphology with nanopores among them. The surface of $CuFe_2O_4$ is smooth and the inter-planar sapcing of 0.248 nm in Figure 2b is ascribed to the (400) crystal plane of $CuFe_2O_4$. For $CuFe_2O_4$@$CeO_{2-\delta}$-0.025 (Figure 2c and Figure 2d), there are amorphous $CeO_{2-\delta}$ nanoclusters on the surface of $CuFe_2O_4$. For $CuFe_2O_4$@$CeO_{2-\delta}$-0.05, the sample maintains the morphology of $CuFe_2O_4$ but there are some $CeO_{2-\delta}$ nanocrystals with size of around 5 nm on the surface of $CuFe_2O_4$ particles, as shown in Figure 2e and Figure 2f. The inter-planar spacing of 0.251 nm in Figure 2f is corresponding to the (200) crystal plane of $CeO_{2-\delta}$ while the inter-planar spacing of 0.233 nm in Figure 2f can be ascribed to the (222) crystal plane of $CuFe_2O_4$, as shown in the HRTEM image (Figure 2f). With further increase of Ce amount, i.e. $CuFe_2O_4$@$CeO_{2-\delta}$-0.10 displays increased $CeO_{2-\delta}$ nanoparticles on its surface (Figure 2g and Figure 2f).

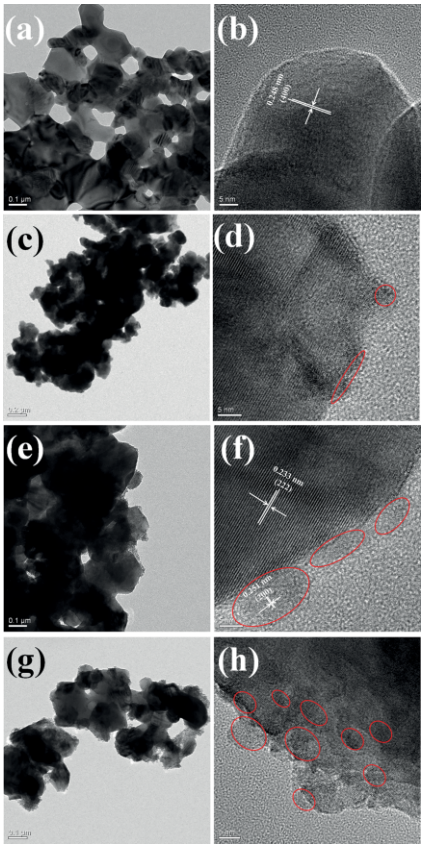

Figure 2. TEM and HRTEM images: (a, b) $CuFe_2O_4$, (c, d) $CuFe_2O_4$@$CeO_{2-\delta}$-0.025, (e, f) $CuFe_2O_4$@$CeO_{2-\delta}$-0.05, (g, h) $CuFe_2O_4$@$CeO_{2-\delta}$-0.10. The red circles are $CeO_{2-\delta}$ nanocrystals on the surface of $CuFe_2O_4$.

The FESEM images of $CuFe_2O_4$ and $CuFe_2O_4$@$CeO_{2-\delta}$-*x* samples shown in Figure 3 also clearly show the nanoparticle morphology of $CuFe_2O_4$ with nanopores among them (Figure 3a) but the surface modification of $CeO_{2-\delta}$ nanocrystals was not obvious for $CuFe_2O_4$@$CeO_{2-\delta}$-0.25 (Figure 3b) due to its small particle size. With the increasing Ce content, there are some $CeO_{2-\delta}$ nanoparticles observed on the surface of $CuFe_2O_4$ in $CuFe_2O_4$@$CeO_{2-\delta}$-0.05 (Figure 3c) and $CuFe_2O_4$@$CeO_{2-\delta}$-0.10 (Figure 3d), consistent with the TEM results. The BET surface

areas of $CuFe_2O_4$, $CuFe_2O_4$@$CeO_{2-\delta}$-0.025, $CuFe_2O_4$@$CeO_{2-\delta}$-0.05 and $CuFe_2O_4$@$CeO_{2-\delta}$-0.10 samples are 16.3, 28.2, 38.8 and 43.8 m^2/g, respectively, indicating the surface modification of $CeO_{2-\delta}$ nanocrystals would lead to increased surface areas due to the much smaller size of $CeO_{2-\delta}$ nanocrystals than that of $CuFe_2O_4$ particles.

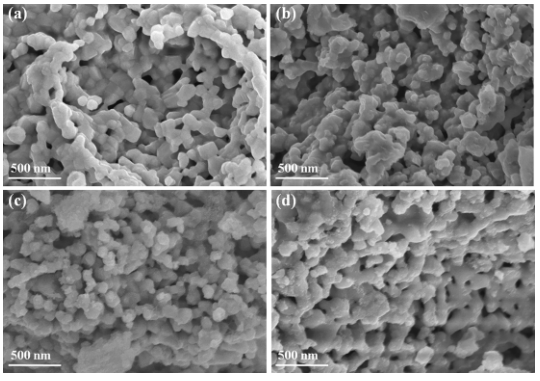

Figure 3. FESEM images (a) $CuFe_2O_4$, (b) $CuFe_2O_4$@$CeO_{2-\delta}$-0.025, (c) $CuFe_2O_4$@$CeO_{2-\delta}$-0.05, and (d) $CuFe_2O_4$@$CeO_{2-\delta}$-0.10.

The oxidation states of copper and iron in the $CuFe_2O_4$ and $CuFe_2O_4$@$CeO_{2-\delta}$-*x* samples were determined via X-ray photoelectron spectroscopy (XPS) analysis. The XPS survery spectrum shows the coexistence of Cu, Fe, O and Ce (Figure 4a). The deconvoluted Cu 2p XPS spectrum of $CuFe_2O_4$@$CeO_{2-\delta}$-0.05 is shown in Figure 4b. The "shake-up" satellites at 941.7 eV and 961.8 eV in the Cu 2p XPS spectrum (Figure 4a) are characteristic for Cu^{2+}, confirming the presence of Cu^{2+}.[15] Several literatures have reported different results for the Cu XPS spectrum in spinel-type $CuFe_2O_4$, some containing only Cu^{2+}[3e,3f,18] while some containing both Cu^{2+} and Cu^{+}.[19] In order to determine the valences of Cu species in $CuFe_2O_4$ and $CuFe_2O_4$@$CeO_{2-\delta}$-*x* samples, the oxidation state of Cu was further confirmed by LMM Auger electron spectroscopy mesurement (Figure 4c). The detection of the peak at 568.9 eV corresponds to Cu^{2+}, which is lower than that of Cu_2O (570.1 eV), indicating that only Cu^{2+} was existed in $CuFe_2O_4$@$CeO_{2-\delta}$-0.05.[20] The Fe 2p spectrum in Figure 4d displays two main spin–orbit lines of $2p_{3/2}$ at around 710.9 eV and $2p_{1/2}$ at around 724.4 eV. The satellite peaks at around 719.1 eV and 733.4 eV show the Fe^{3+} state in $CuFe_2O_4$@$CeO_{2-\delta}$-0.05. The deconvoluted Ce 3d spectra (Figure 4e) of $CuFe_2O_4$@$CeO_{2-\delta}$-0.05 include four main spin-orbit doublets, indicating the co-existence of Ce^{3+} and Ce^{4+}. The main peak at around 529.8 eV in the O 1s spectra can be attributed to the characteristic oxygen peak (O^{2-}) of metal oxides while the shoulder with the binding energy around 531.5 eV represents the chemisorbed surface oxygen species such as O_2^- and O^- with low coordination (Figure 4f). All the Cu 2p and Fe 2p in $CuFe_2O_4$, $CuFe_2O_4$@$CeO_{2-\delta}$-0.025 and $CuFe_2O_4$@$CeO_{2-\delta}$-0.10 exhibited similar spectrum to that of $CuFe_2O_4$@$CeO_{2-\delta}$-0.05, as shown in Figure 5a and Figure 5b, respectively. In addition, the Ce 3d XPS spectra of $CuFe_2O_4$@$CeO_{2-\delta}$-0.025 and $CuFe_2O_4$@$CeO_{2-\delta}$-0.10 can also be deconvoluted into four main spin-orbit doublets, as shown in Figure 5c and Figure 5d respectively. The molar ratios of Ce^{3+}/Ce^{4+} were calculated from the surface area of deconvoluted peaks. With the increment of $CeO_{2-\delta}$ modification amount, the molar ratio of Ce^{3+}/Ce^{4+} decreased slightly from 0.32 for $CuFe_2O_4$@$CeO_{2-\delta}$-0.025 to 0.28 for $CuFe_2O_4$@$CeO_{2-\delta}$-0.10. Finally, the coexistence of Cu^{2+}, Fe^{3+} and Ce^{3+}/Ce^{4+} redox couples would favor the oxygen ion mobility and may enhance the catalytic activity.

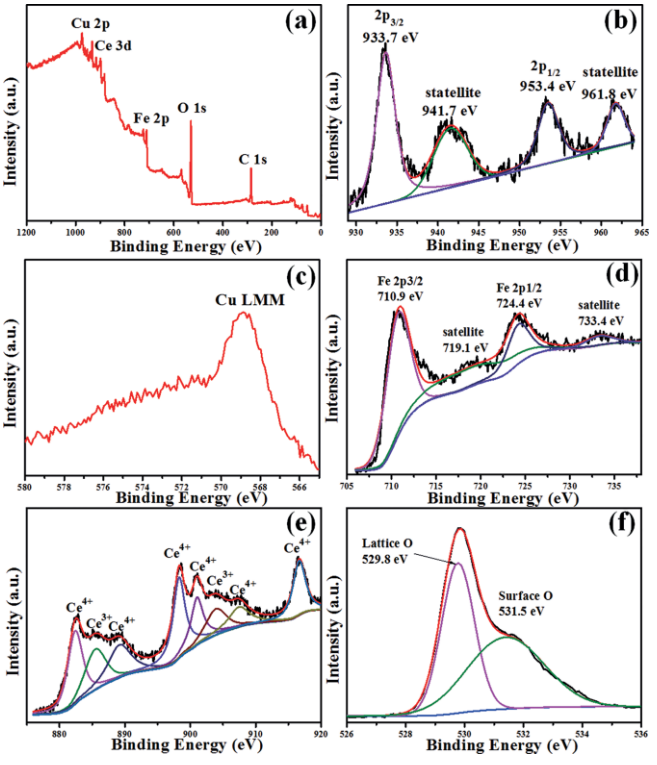

Figure 4. XPS spectra of $CuFe_2O_4$@$CeO_{2-\delta}$-0.05 sample: (a) survey spectrum, (b) Cu 2p, (c) Cu LMM AES, (d) Fe 2p, (e) Ce 3d and (f) O 1s.

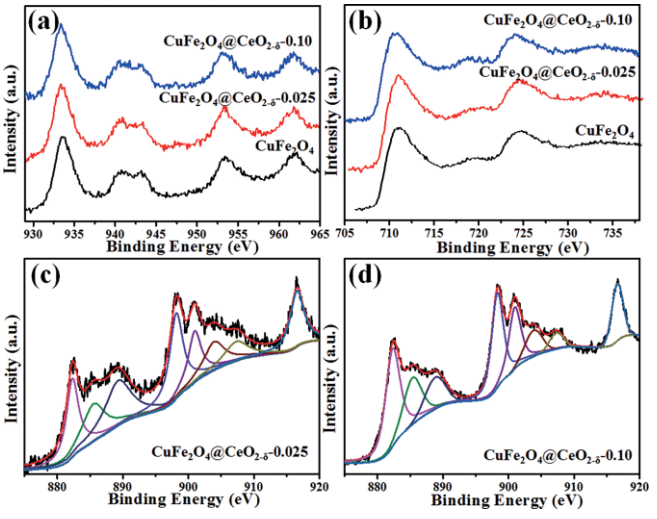

Figure 5. XPS spectra of as-synthesized samples: (a) Cu 2p, (b) Fe 2p, and (c, d) Ce 3d.

Temperature-programmed reduction (H_2-TPR) profiles of $CuFe_2O_4$, $CuFe_2O_4$@$CeO_{2-\delta}$-*x* samples and $CeO_{2-\delta}$ under flowing 5 %H_2/95 %N_2 are shown in Figure 6. In the cases of $CuFe_2O_4$ and $CuFe_2O_4$@$CeO_{2-\delta}$-*x* samples, the sharp peak starting from 110 °C with maximum at 195 °C can be ascribed to the reduc-

tion of $CuFe_2O_4$ to Cu and Fe_3O_4 phases, and the reduction at higher temperature from 270 °C to 550 °C with maximum at around 440 °C is attributed to the further reduction of Fe_3O_4 to form metallic Fe.[21] Compared with pure $CuFe_2O_4$, the $CuFe_2O_4$@$CeO_{2-\delta}$-*x* samples exhibit a bit lower reduction temperature even though the reduction temperatures for pure $CeO_{2-\delta}$ are 432 and 699 °C, which can be ascribed to the synergetic effect between $CuFe_2O_4$ and $CeO_{2-\delta}$ for the enhanced oxygen transfer properties.[17c,22] The lower reduction temperatures, especially $CuFe_2O_4$@$CeO_{2-\delta}$-0.05 than that of pure $CuFe_2O_4$ indicate their higher oxygen removal ability and potential catalytic activity at low temperatures.[17a]

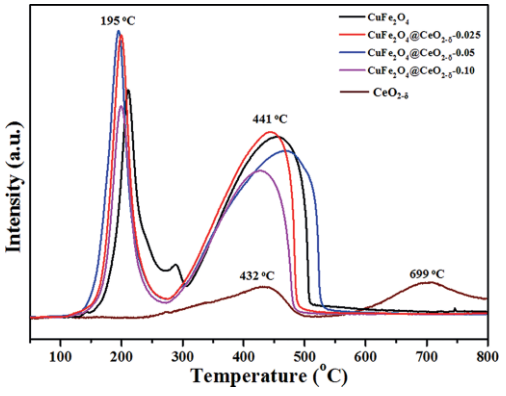

Figure 6. H_2-TPR profiles of $CuFe_2O_4$, $CuFe_2O_4$@$CeO_{2-\delta}$-*x* and $CeO_{2-\delta}$. Catalyst weight 0.10 g; gas composition 5 %H_2/95 %N_2 balance; flow rate 30 mL min^{-1}; temperature ramp 10 K min^{-1}.

The catalytic activities of as-prepared samples were evaluated by the synthesis of fluorenone at 60 °C under air atmosphere using NHPI, which has been found to efficiently catalyze the aerobic oxidation of organic substrates via the formation of radicals from NHPI and O_2 at high temperature (e.g., 100 °C). Initially, the catalytic activity of as-prepared materials was investigated at 60 °C under air for 24 h (Entries 1–7 in Table 1). Only fluorenone was detected as the products during the catalytic reaction, indicating the excellent selectivity. Pure $CuFe_2O_4$ exhibited an 64 % conversion (Entry 1, Table 1). With 2.65 wt.-% Ce modification amount in $CuFe_2O_4$@$CeO_{2-\delta}$-0.025, the conversion of fluorene increased to 82 % (Entry 2, Table 1). Further increasing Ce modification amount to 4.20 wt.-% in $CuFe_2O_4$@$CeO_{2-\delta}$-0.05 would lead to a higher conversion, reaching 94 % (Entry 3, Table 1). Nevertheless, $CuFe_2O_4$@$CeO_{2-\delta}$-0.10 with 8.76 wt.-% Ce exhibited a worse catalytic performance with only 81 % conversion (Entry 4, Table 1), suggesting too much $CeO_{2-\delta}$ coated on the surface would reduce the available active sites on $CuFe_2O_4$. In addition, the inferior catalytic activities of CuO (Entry 6, Table 1) and Fe_2O_3 (Entry 7, Table 1) than those of $CuFe_2O_4$ and $CuFe_2O_4$@$CeO_{2-\delta}$-*x* demonstrate the synergetic effect between Cu species and Fe species in $CuFe_2O_4$. Even though NHPI itself was reported as active catalyst in the oxidation of fluorene, the activation temperature and oxygen pressure are usually high (e.g., 100 °C under 1 atm O_2).[23] At 60 °C under air atmosphere for 24 h, the activity of NHPI for our system is only 36 % conversion (Entry 8, Table 1), suggesting that the addition of transition metal oxide catalysts can accelerate the generation of phthalimide-*N*-oxyl (PINO) radical from NHPI and O_2 to abstract a hydrogen from fluorene with the formation of alkyl radicals, which were converted into ketones by the peroxy radicals.[23]

Table 1. Catalytic performance over as-prepared catalysts.

Entry	Catalyst[a]	Conv. (%)[e]	Select. (%)[e]
1	$CuFe_2O_4$	64	>99
2	$CuFe_2O_4$@$CeO_{2-\delta}$-0.025	82	>99
3	$CuFe_2O_4$@$CeO_{2-\delta}$-0.05	94	>99
4	$CuFe_2O_4$@$CeO_{2-\delta}$-0.10	81	>99
5	$CeO_{2-\delta}$	trace	>99
6	CuO	39	>99
7	Fe_2O_3	40	>99
8	NHPI	36	>99
9[b]	$CuFe_2O_4$@@$CeO_{2-\delta}$-0.05	90	>99
10[c]	$CuFe_2O_4$@@$CeO_{2-\delta}$-0.05	74	>99
11[d]	$CuFe_2O_4$@@$CeO_{2-\delta}$-0.05	77	>99
12	2nd $CuFe_2O_4$@$CeO_{2-\delta}$-0.05	91	>99
13	3rd $CuFe_2O_4$@$CeO_{2-\delta}$-0.05	90	>99
14	4th $CuFe_2O_4$@@$CeO_{2-\delta}$-0.05	88	>99
15	5th $CuFe_2O_4$@@$CeO_{2-\delta}$-0.05	87	>99

[a] Catalytic conditions: fluorene (1.0 mmol), 20 mg of catalyst (other catalysts with the same Cu or Fe content of $CuFe_2O_4$@$CeO_{2-\delta}$-0.05), NHPI, 0.1 mmol, CH_3CN (5.0 mL), 60 °C, air atmosphere, 24 h. [b] 20 mg catalyst, 50 °C, 24 h. [c] 20 mg catalyst, 70 °C, 24 h. [d] 10 mg catalyst, 60 °C, 24 h. [e] Conversion and selectivity were calculated by GC/MS using nitrobenzene as internal standard.

In addition, the reaction temperature also has great influence on the catalytic performance (Entries 9–10, Table 1), in which there is 90 % conversion at 50 °C for 24 h while only 74 % conversion at 70 °C for 24 h. It is observed during the catalytic tests that most of $CuFe_2O_4$@$CeO_{2-\delta}$-0.05 is adhered on the surface of glass reactor at 70 °C. When 10 mg of $CuFe_2O_4$@$CeO_{2-\delta}$-0.05 was used as catalyst, the conversion of fluorene was 77 % at 60 °C for 24 h (Entry 11, Table 1). All the results suggest that $CeO_{2-\delta}$ modification with suitable content on $CuFe_2O_4$ nanoparticles would increase the catalytic activity even though pure $CeO_{2-\delta}$ almost had no activity for the selective oxidation of fluorene (Entry 5, Table 1). It is anticipated that $CeO_{2-\delta}$ nanocrystals with Ce^{3+}/Ce^{4+} may react with PINO radicals quickly, resulting in very poor activity. To illustrate the excellent activity of $CuFe_2O_4$@$CeO_{2-\delta}$-0.05 in our work, the activities of other reported catalysts were summarized in Table 2 as comparison. It obviously shows the superviour or comparable

Table 2. Catalytic performance over various catalysts.

No	Catalyst	Reaction conditions	Yield (%)	Ref.
1	$CuFe_2O_4$@$CeO_{2-\delta}$-0.05	20 mg catalyst, air, 60 °C, NHPI, 24 h	94	This work
2	$Pd/SnBi3_{SG}$	100 mg catalyst, O_2 flusing, UV light, 60 mW cm^{-2}, 6 h	72	[24]
3	Iron(III) complex of tridentate ligand	2×10^{-4} mM catalyst, 150eq H_2O_2, 40 °C, 48 h	25	[25]
4	Cu-$CuFe_2O_4$@HKUST-1	15 mg catalyst, 1 atm O_2, 60 °C, NHPI, 9 h	99	[16b]
5	Pd-POVs	3.75 μmol catalyst, 2.5 equiv. TBHP, 65 °C, 16 h	99	[26]

activity of $CuFe_2O_4$@$CeO_{2-\delta}$-0.05 under mild conditions with the reported values using strong oxidants or noble metals.

Based on the aforementioned results, a reaction mechanism was proposed, as displayed in Figure 7. NHPI was first initiated by Cu^{2+} and/or Fe^{3+} in $CuFe_2O_4$@$CeO_{2-\delta}$-*x* samples to form PINO, which will then withdraw a hydrogen from fluorene to form NHPI and a benzylic carbon radical. When $CuFe_2O_4$ nanoparticles were modified with sutiable $CeO_{2-\delta}$ nanocrystals, the formed Cu^+ or Fe^{2+} intermediates will be re-oxidized by adsorbed oxygen on $CeO_{2-\delta}$ nanocrystals. In addition, the adsorbed O_2 by $CeO_{2-\delta}$ will oxidize the benzylic carbon radicals to finally form fluorenone.

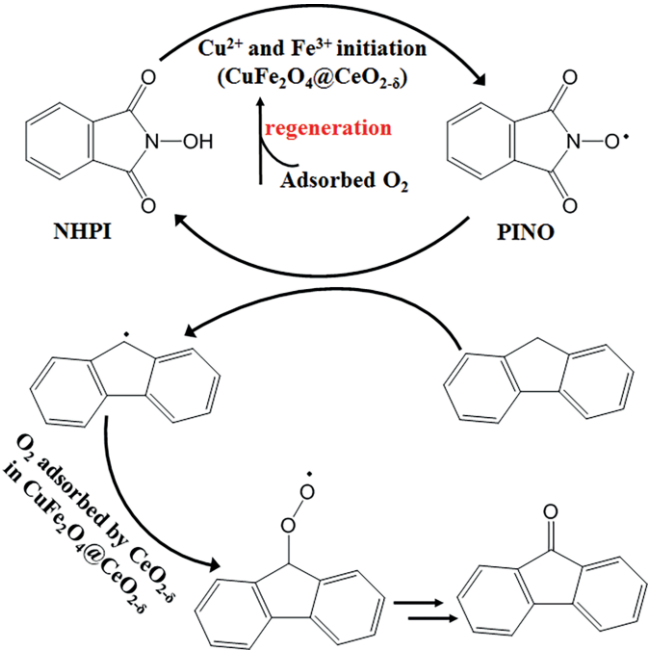

Figure 7. Proposed reaction mechanism of selective oxidation of fluorene in the presence of NHPI and $CuFe_2O_4$@$CeO_{2-\delta}$-*x* samples under air atmosphere.

To illustrate the reusability test, $CuFe_2O_4$@$CeO_{2-\delta}$-0.05 was chosen as the catalyst. After each catalytic test, $CuFe_2O_4$@$CeO_{2-\delta}$-0.05 was collected by a magnet and washing with ethanol three times to remove the products, followed by drying at 70 °C under vacuum for 12 h. The catalytic activity for five cycling times was summarized in Entries 12–15 of Table 1. There is only a slight decrease in the conversion due to the loss of some catalysts during the recycling process, indicating the good reusability of $CuFe_2O_4$@$CeO_{2-\delta}$-0.05. In addition, the collected liquid after the 1st cycling catalytic test was investigated by employing the ICP-AES analysis and only trace losses of Cu (6 %), Fe (2 %) and Ce (4 %) ions were detected, indicating the relatively good stability of $CuFe_2O_4$@$CeO_{2-\delta}$-0.05. The similar Cu LMM AES (Figure 8a), Fe 2p (Figure 8b) spectrum and XRD pattern (Figure 8d) of fresh and the 1st used $CuFe_2O_4$@$CeO_{2-\delta}$-0.05 also demonstrated its good stability of $CuFe_2O_4$ in $CuFe_2O_4$@$CeO_{2-\delta}$-0.05 during the catalytic test. The slightly reduced intensity of Cu LMM, Fe 2p and Ce 3d (Figure 8) indicated the loss of trace $CuFe_2O_4$ and $CeO_{2-\delta}$ nanocrystals during the catalytic process, which may attribute to the slightly decreased conversion for the cycling test.

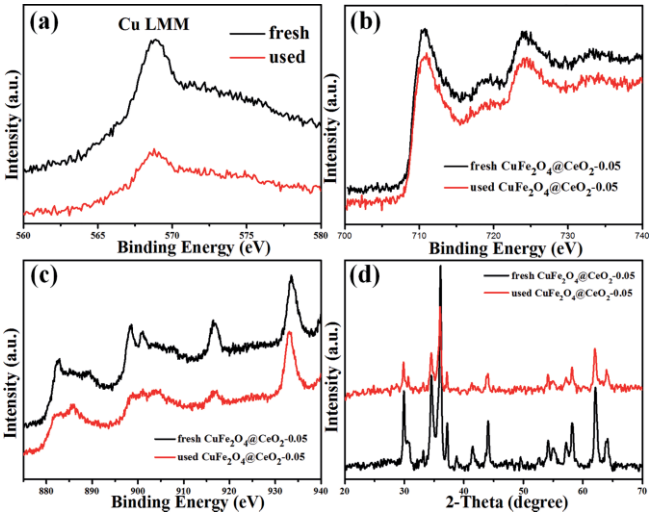

Figure 8. (a) Cu LMM AES, (b) Fe 2p XPS spectra, (c) Ce 3d XPS spectra and (d) XRD patterns of fresh and used $CuFe_2O_4$@$CeO_{2-\delta}$-0.05.

Conclusions

In summary, we have prepared a series of $CeO_{2-\delta}$-modified $CuFe_2O_4$ with a controlled amount of $CeO_{2-\delta}$ and enhanced oxygen transfer properties. The catalytic results in the selective oxidation of the sp^3 C–H bond in an air atmosphere at 60 °C demonstrate that the surface modification of $CeO_{2-\delta}$ with the optimized amount (i.e., 4.20 wt.-% Ce in our work) improves the conversion of fluorene from 64 % for $CuFe_2O_4$ to 94 % for $CuFe_2O_4$@$CeO_{2-\delta}$-0.05 even though the $CeO_{2-\delta}$ itself has no activity in our catalytic system. The improved catalytic performance can be attributed to the enhanced reductivity and oxygen transfer of $CuFe_2O_4$ arising from the synergetic effect between $CuFe_2O_4$ and $CeO_{2-\delta}$, as demonstrated by the XPS and TPR results. Our results could lead to the design of efficient catalysts in organic synthesis based on spinels (e.g., $CuFe_2O_4$) via surface modification with the best synergetic effects.

Experimental Section

Sample Preparation

Synthesis of $CuFe_2O_4$ Nanoparticles: The $CuFe_2O_4$ nanoparticles were by a sol-gel combustion method.[18b] Typically, 10 mmol of $Cu(NO_3)_2$·$3H_2O$ (Alfa Aesar, 98 %), 20 mmol of $Fe(NO_3)_3$·$9H_2O$ (Alfa Aesar, 98 %) and 60 mmol of citric acid were dissolved in 100 mL of deionized water under continuous stirring for 2 h. After the evaporation of solvent at 100 °C, the obtained dried precursor was further combusted at 200 °C and then calcined at 700 °C for 4 h.

Synthesis of $CuFe_2O_4$@$CeO_{2-\delta}$: The $CeO_{2-\delta}$ modified $CuFe_2O_4$ samples were synthesized according to our previous work.[17c] In a typical process, 0.30 g of $CuFe_2O_4$ was added in the mixture of 60 mL of H_2O and 60 mL of ethanol. After ultrasonication for 30 min and stirring for 2 h, 0.025, 0.05, or 0.10 g of $Ce(NO_3)_3$·$6H_2O$ (99 %, Sigma–Aldrich) was added into the above solution. After another 3 h whilst stirring, the pH of the solution was adjusted to around 11 by 25–28 wt.-% NH_3·H_2O. After 3 h, the solid was separated by centrifugation, washed with H_2O and ethanol for several times. After dried at 80 °C for 12 h, the final products were obtained by

calcined at 300 °C under static air for 2 h. The final products were referred as $CuFe_2O_4$@$CeO_{2-\delta}$-*x*, in which *x* is the weight of added $Ce(NO_3)_3{\cdot}6H_2O$ in g.

Characterization

Powder X-ray diffraction (XRD) patterns were obtained at room temperature on a M21X X-ray Diffractometer with Cu-K_α irradiation (λ = 1.541 Å). The morphologies of all samples were observed on a ZEISS SUPRA55 instrument operated at an acceleration voltage of 10 kV. High-resolution transmission electron microscopy (HRTEM) images were obtained on a JEM2100F operated at the accelerating voltages of 200 kV. Nitrogen adsorption-desorption isotherms were measured at 77 K. Each sample (100 mg) was degassed at 150 °C for 6 h under vacuum before an adsorption measurement. The Brunauer-Emmett-Teller (BET) method was utilized to calculate the specific surface areas. X-ray photoelectron spectroscopy (XPS) data were obtained on a Thermo ESCALAB 250Xi spectrophotometer with LMM Auger electron spectroscopy (AES) using 150 W Al Kα radiation and for peak calibration adventitious C 1s was set at 284.9 eV. Temperature-programmed reduction with H_2 (H_2-TPR) was performed on a Micromeritics ASAP-2020 analyzer (Micromeritics Instrument Corp., USA. In the H_2-TPR measurements, catalyst samples were heated at a rate of 10 K min^{-1} from 50 to 800 °C under 5 %H_2/95 %N_2 with a flowing rate of 30 mL/min. The Ce contents of the samples and the liquid after the catalytic test were obtained using inductively coupled plasma-atomic emission spectrometry (ICP-AES).

Catalyst Test

The oxidation reaction was carried out in a 50 mL round-bottom flask fitted with a water condenser. Typically, 20 mg of catalyst, fluorene (1.0 mmol), and N-hydroxyphthalimide (NHPI) (0.1 mmol) were dispersed in 5 mL of acetonitrile at 60 °C under vigorous stirring under atmosphere pressure. After reaction for certain time, the catalyst was separated with the liquid by centrifugation and the liquid samples were analyzed using gas chromatography-mass spectrometry (GC–MS, Agilent 7890/5975C-GC/MSD) with an HP-5 capillary column using nitrobenzene as an internal stand. Products were also identified using standard compounds and comparing the retention time. For better accuracy, their average activity was calculated from GC–MS test results for three times. For the reusability, the catalyst was collected by a magnet, washed with ethanol three times to remove the products and dried at 70 °C under vacuum for 12 h. After this treatment, the obtained catalyst was tested for the second time reaction.

Acknowledgments

The authors are grateful for financial support from the National Natural Science Foundation of China (51802015), the Key Research Program of China (2018YFB0605900), the Fundamental Research Funds for the Central Universities (FRF-BD-17-013A), and the Beijing Organization Department (Program of Young Scholar 2017000020124G090).

Keywords: Heterogeneous catalysis · Nanoparticles · O-O activation · Oxidation · Oxygen transfer

[1] a) Y.-J. Liu, H. Xu, W.-J. Kong, M. Shang, H.-X. Dai, J.-Q. Yu, *Nature* **2014**, *515*, 389; b) C. Yuan, Y. Liang, T. Hernandez, A. Berriochoa, K. N. Houk, D. Siegel, *Nature* **2013**, *499*, 192.

[2] a) S. M. Silvestre, J. A. R. Salvador, *Tetrahedron* **2007**, *63*, 2439–2445; b) K. Gardner, J. Mayer, *Science* **1995**, *269*, 1849–1851.

[3] a) D.-S. Kim, W.-J. Park, C.-H. Jun, *Chem. Rev.* **2017**, *117*, 8977–9015; b) E. Roduner, W. Kaim, B. Sarkar, V. B. Urlacher, J. Pleiss, R. Gläser, W. D. Einicke, G. A. Sprenger, U. Beifuß, E. Klemm, C. Liebner, H. Hieronymus, S. F. Hsu, B. Plietker, S. Laschat, *ChemCatChem* **2013**, *5*, 82–112; c) T. Newhouse, P. S. Baran, *Angew. Chem. Int. Ed.* **2011**, *50*, 3362–3374; *Angew. Chem.* **2011**, *123*, 3422; d) X. Huang, J. Li, G. Shen, N. Xin, Z. Lin, Y. Chi, J. Dou, D. Li, C. Hu, *Dalton Trans.* **2018**, *47*, 726–733; e) L. M. D. R. S. Martins, A. J. L. Pombeiro, *Eur. J. Inorg. Chem.* **2016**, *2016*, 2236–2252; f) L. M. D. R. S. Martins, A. J. L. Pombeiro, *Coord. Chem. Rev.* **2014**, *265*, 74–88.

[4] X. Huang, G. Zhao, P. Wang, H. Zheng, W. Dong, G. Wang, *ChemCatChem* **2018**, *10*, 1406–1413.

[5] a) J. Wang, S. Fan, Y. Luan, J. Tang, Z. Jin, M. Yang, Y. Lu, *RSC Adv.* **2015**, *5*, 2405–2410; b) S. S. Acharyya, S. Ghosh, N. Siddiqui, L. N. Sivakumar Konathala, R. Bal, *RSC Adv.* **2015**, *5*, 4838–4843; c) S. S. Acharyya, S. Ghosh, S. Adak, D. Tripathi, R. Bal, *Catal. Commun.* **2015**, *59*, 145–150.

[6] a) C.-C. Liu, R. Ramu, S. I. Chan, C.-Y. Mou, S. S. F. Yu, *Catal. Sci. Technol.* **2016**, *6*, 7623–7630; b) A. Santiago-Portillo, S. Navalón, F. G. Cirujano, F. X. L. i. Xamena, M. Alvaro, H. Garcia, *ACS Catal.* **2015**, *5*, 3216–3224; c) X. Lin, Z. Nie, L. Zhang, S. Mei, Y. Chen, B. Zhang, R. Zhu, Z. Liu, *Green Chem.* **2017**, *19*, 2164–2173; d) Y. Wang, J. Zhang, X. Wang, M. Antonietti, H. Li, *Angew. Chem. Int. Ed.* **2010**, *49*, 3356–3359; *Angew. Chem.* **2010**, *122*, 3428; e) X.-H. Li, X. Wang, M. Antonietti, *ACS Catal.* **2012**, *2*, 2082–2086.

[7] P. Zhang, H. Lu, Y. Zhou, L. Zhang, Z. Wu, S. Yang, H. Shi, Q. Zhu, Y. Chen, S. Dai, *Nat. Commun.* **2015**, *6*, 8446.

[8] L. Kesavan, R. Tiruvalam, M. H. A. Rahim, M. I. bin Saiman, D. I. Enache, R. L. Jenkins, N. Dimitratos, J. A. Lopez-Sanchez, S. H. Taylor, D. W. Knight, C. J. Kiely, G. J. Hutchings, *Science* **2011**, *331*, 195–199.

[9] a) Y. Zhang, N. Zhang, Z.-R. Tang, Y.-J. Xu, *Chem. Sci.* **2012**, *3*, 2812–2822; b) M.-Q. Yang, Y. Zhang, N. Zhang, Z.-R. Tang, Y.-J. Xu, *Sci. Rep.* **2013**, *3*, 3314.

[10] S. Verma, R. B. Nasir Baig, M. N. Nadagouda, R. S. Varma, *ACS Sustainable Chem. Eng.* **2016**, *4*, 2333–2336.

[11] S. A. Kondrat, T. E. Davies, Z. L. Zu, P. Boldrin, J. K. Bartley, A. F. Carley, S. H. Taylor, M. J. Rosseinsky, G. J. Hutchings, *J. Catal.* **2011**, *281*, 279–289.

[12] X. Huang, L. Liu, H. Gao, W. Dong, M. Yang, G. Wang, *Green Chem.* **2017**, *19*, 769–777.

[13] a) H. C. Genuino, S. Dharmarathna, E. C. Njagi, M. C. Mei, S. L. Suib, *J. Phys. Chem. C* **2012**, *116*, 12066–12078; b) E. C. Njagi, H. C. Genuino, C. K. King'ondu, S. Dharmarathna, S. L. Suib, *Appl. Catal. A* **2012**, *421*, 154–160; c) B. Solsona, T. Garcia, S. Agouram, G. J. Hutchings, S. H. Taylor, *Appl. Catal. B* **2011**, *101*, 388–396.

[14] R. Zhang, J. Liu, S. Wang, J. Niu, C. Xia, W. Sun, *ChemCatChem* **2011**, *3*, 146–149.

[15] J. Papavasiliou, G. Avgouropoulos, T. Ioannides, *J. Catal.* **2007**, *251*, 7–20.

[16] a) S. S. Acharyya, S. Ghosh, R. Tiwari, C. Pendem, T. Sasaki, R. Bal, *ACS Catal.* **2015**, *5*, 2850–2858; b) S. Fan, W. Dong, X. Huang, H. Gao, J. Wang, Z. Jin, J. Tang, G. Wang, *ACS Catal.* **2017**, *7*, 243–249.

[17] a) F. Wang, X. Wang, D. Liu, J. Zhen, J. Li, Y. Wang, H. Zhang, *ACS Appl. Mater. Interfaces* **2014**, *6*, 22216–22223; b) X. Huang, C. Ni, G. Zhao, J. T. S. Irvine, *J. Mater. Chem. A* **2015**, *3*, 12958–12964; c) X. Huang, G. Zhao, Y. Chang, G. Wang, J. T. S. Irvine, *Appl. Surf. Sci.* **2018**, *440*, 20–28; d) X. Wang, S. Zhao, Y. Zhang, Z. Wang, J. Feng, S. Song, H. Zhang, *Chem. Sci.* **2016**, *7*, 1109–1114; e) W.-W. Wang, W.-Z. Yu, P.-P. Du, H. Xu, Z. Jin, R. Si, C. Ma, S. Shi, C.-J. Jia, C.-H. Yan, *ACS Catal.* **2017**, *7*, 1313–1329; f) X. Han, C. Li, X. Liu, Q. Xia, Y. Wang, *Green Chem.* **2017**, *19*, 996–1004; g) R. Palacio, S. Torres, S. Royer, A. S. Mamede, D. Lopez, D. Hernandez, *Dalton Trans.* **2018**, *47*, 4572–4582.

[18] a) X. Zhang, M. Feng, R. Qu, H. Liu, L. Wang, Z. Wang, *Chem. Eng. J.* **2016**, *301*, 1–11; b) C. Luadthong, P. Khemthong, W. Nualpaeng, K. Faungnawakij, *Appl. Catal. A* **2016**, *525*, 68–75.

[19] P. Jing, J. Li, L. Pan, J. Wang, X. Sun, Q. Liu, *J. Hazard. Mater.* **2015**, *284*, 163–170.

[20] a) S. Poulston, P. M. Parlett, P. Stone, M. Bowker, *Surf. Interface Anal.* **1996**, *24*, 811–820; b) L. Martin, H. Martinez, D. Poinot, B. Pecquenard, F. Le Cras, *J. Phys. Chem. C* **2013**, *117*, 4421–4430.

[21] K. Faungnawakij, R. Kikuchi, T. Fukunaga, K. Eguchi, *Catal. Today* **2008**, *138*, 157–161.

[22] Y. Xiao, W. Zhao, K. Zhang, Y. Zhang, X. Wang, T. Zhang, X. Wu, C. Chen, L. Jiang, *Dalton Trans.* **2017**, *46*, 16967–16972.
[23] Y. Ishii, K. Nakayama, M. Takeno, S. Sakaguchi, T. Iwahama, Y. Nishiyama, *J. Org. Chem.* **1995**, *60*, 3934–3935.
[24] M. M. Mohamed, S. A. Ahmed, *Microporous Mesoporous Mater.* **2015**, *204*, 62–72.
[25] N. Tyagi, O. Singh, K. Ghosh, *Catal. Commun.* **2017**, *95*, 83–87.
[26] J.-K. Li, X.-Q. Huang, S. Yang, H.-W. Ma, Y.-N. Chi, C.-W. Hu, *Inorg. Chem.* **2015**, *54*, 1454–1461.

Received: November 8, 2018

Nanoparticles for Oxygen Transfer

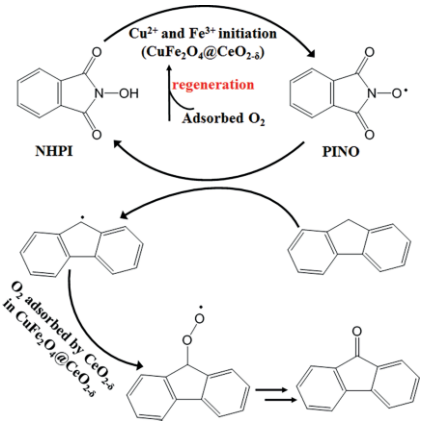

$CeO_{2-\delta}$ modification with 4.20 wt.-% Ce on the surface of $CuFe_2O_4$ nanoparticles favors oxygen transfer at lower temperature and leads to better catalytic activity than that of pure $CuFe_2O_4$ for the aerobic selective oxidation of fluorene due to the synergetic effect between $CuFe_2O_4$ and $CeO_{2-\delta}$ with Ce^{3+}/Ce^{4+}.

DOI: 10.1002/ejic.201801374